Published in final edited form as:
Cancer Res. 2013 August 15; 73(16): 5003–5015. doi:10.1158/0008-5472.CAN-12-1597.

Myeloid derived suppressor cells as a vehicle for tumor-specific oncolytic viral therapy

Samuel Eisenstein[1,2], **Brian A. Coakley**[1,2,#], **Karen Briley-Saebo**[3,#], **Ge Ma**[1], **Marcia Meseck**[4], **Stephen Ward**[5], **Celia Divino**[2], **Savio Woo**[4], **Shu-Hsia Chen**[1,2,6,7], and **Ping-Ying Pan**[1,6]

[1]Department of Oncological Sciences, Mount Sinai School of Medicine, 1425 Madison Avenue, Room 13-76, New York, NY 10029-6574

[2]Department of Surgery, Mount Sinai School of Medicine, 1425 Madison Avenue, Room 13-76, New York, NY 10029-6574

[3]Department of Radiology, Mount Sinai School of Medicine, 1425 Madison Avenue, Room 13-76, New York, NY 10029-6574

[4]Department of Medicine, Mount Sinai School of Medicine, 1425 Madison Avenue, Room 13-76, New York, NY 10029-6574

[5]Department of Pathology, Mount Sinai School of Medicine, 1425 Madison Avenue, Room 13-76, New York, NY 10029-6574

[6]Immunology Institute, Mount Sinai School of Medicine, 1425 Madison Avenue, Room 13-76, New York, NY 10029-6574

[7]Tisch Cancer Institute, Mount Sinai School of Medicine, 1425 Madison Avenue, Room 13-76, New York, NY 10029-6574

Abstract

One of the several impediments to effective oncolytic virus therapy of cancer remains a lack of tumor-specific targeting. Myeloid derived suppressor cells (MDSCs) are immature myeloid cells induced by tumor factors in tumor-bearing hosts. The biodistribution kinetics of MDSC and other immune cell types in a murine hepatic colon cancer model was investigated through the use of tracking markers and magnetic resonance imaging (MRI). MDSCs were superior to other immune cell types in preferential migration to tumors in comparison to other tissues. Based on this observation, we engineered a strain of vesicular stomatitis virus (VSV), an oncolytic rhabdovirus, that bound MDSCs and used them as a delivery vehicle. Improving VSV binding efficiency to MDSCs extended the long-term survival of mice bearing metastatic colon tumors, compared to systemic administration of wild-type VSV alone. Survival was further extended by multiple injections of the engineered virus without significant toxicity. Notably, direct tumor killing was accentuated by promoting MDSC differentiation towards the classically activated M1-like

Correspondence: Ping-Ying Pan and Shu-Hsia Chen, Department of Oncological sciences, Box 1496, Mount Sinai School of Medicine, One Gustave L. Levy Place, New York, NY 10029; ping-ying.pan@mssm.edu or shu-hsia.chen@mssm.edu.
[#]These authors contributed equally.

Authorship Statements

Contribution: Samuel Eisenstein, Brian A. Coakley, Karen Briley-Saebo performed most of the research, analyzed data and wrote the manuscript; Ge Ma performed additional research; Marcia Meseck and Savio Woo provided a vital reagent and discussion; Stephen Ward, performed pathology analysis and interpretation. Celia Divino designed research; P.-Y.P. and S.-H.C. designed research and supervised the project and wrote the manuscript with valuable contribution from all other authors.

Conflict-of-interest disclosure: The authors declare no competing financial interests.

phenotype. Our results offer a preclinical proof of concept for using MDSCs to facilitate and enhance the tumor-killing activity of tumor-targeted oncolytic therapeutics.

Introduction

Tumor secreted factors have been shown to promote the abnormal differentiation and accumulation of myeloid progenitor cells, which in turn promote tumor progression and metastases. Myeloid-derived suppressor cells (MDSCs) are a heterogeneous population of immature myeloid cells critical to the development of tumor-induced immune tolerance (1, 2). Classically, they have been described as $CD11b^{+}Gr1^{+}$ cells (3) in murine models, which can be further characterized into monocytic ($Gr1^{Low}ly6G^{-}Ly6C^{High}CD115^{+}$) and granulocytic ($GR1^{High}Ly6G^{+}Ly6C^{Low}CD115^{-}$) subsets (4–6).

MDSCs are enriched when immature myeloid cells develop abnormally in the bone marrow of tumor-bearing hosts (7, 8) at which time MDSCs are released into circulation, accumulating in lymphoid organs (7) and ultimately migrate from these locations to tumors, a process that is mediated by multiple tumor-secreted inflammatory factors, including GM-CSF (6), M-CSF (5), SCF (8), S100A8/A9 (9), VEGF (10), IL-1β (11), and chemokines, e.g. CCL2 (12), CCL5 (our unpublished results). Once MDSCs localize within the tumor microenvironment, they can mediate immune suppression through multiple pathways; i.e. production of arginase (13), inducible nitric oxide synthase (14), reactive oxygen species (15), and suppressive cytokines including IL-10 and TGF-β (5), or via the activation and recruitment of regulatory T cells (Tregs)(5, 16). They also differentiate into more mature, tumor-associated macrophages, which promote angiogenesis and lymphangiogenesis (17, 18).

Vesicular stomatitis virus (VSV) is an oncolytic rhabdovirus that infects mammalian cells. VSV preferentially replicates within and lyses tumor cells due to the tumor cell's inability to mount an appropriate interferon response, which, in normal cells, interferes with viral reproduction, enabling clearance of the virus (19, 20). VSV effectively prolongs survival in mice with metastatic cancer when injected intratumorally (21). A major drawback to this type of therapy in humans is the inability to treat multifocal diseases or inaccessible tumors. While systemic administration of the virus would allow for dissemination to occult metastases, the treatment through systemic injection is limited by toxicity from high doses of VSV (22). Our group and others have observed that these doses lead to neuropathic changes in mammals (22–24).

Due to their unique capability to specifically migrate to tumors, we explore the possibility of employing monocytic, $Ly6C^{+}$ MDSCs (heretofore referred to as MDSCs) as vectors to deliver tumor-specific therapies. Treatments loaded into MDSCs could be directly targeted to the tumor sites, increasing intratumoral, while decreasing extratumoral, dosages, thus preventing systemic side effects and increasing the therapeutic index. We further hypothesize that viral transduced MDSCs can switch from the pro-tumor functional M2 phenotype to antitumor, M1 response, due to viral pathogen mediated inflammatory response. We also demonstrated that MDSCs exhibited much greater tumor-tropism when compared to a variety of other immune cell types (25, 26) and that treatment with VSV-loaded MDSCs, compared to systemic viral therapy, significantly prolonged survival in tumor-bearing mice. This survival benefit was further enhanced through repeated administration of virus-loaded MDSCs. Interestingly, we demonstrated synergistic tumor killing by both the oncolytic virus and the MDSCs themselves, which, after viral interaction, exhibit an M1-like phenotype that promotes tumor killing.

Methods

Experimental animals

BALB/c and C57BL/6 mice were purchased from Jackson Laboratories (Bar Harbor, ME). Animal experiments were performed in accordance with the guidelines of Mount Sinai School of Medicine.

Antibodies and flow cytometry

Anti-Ly6C-FITC, anti-Ly6C-PE, anti-CD11b-APC, anti-Gr-1-PE-Cy5, anti-CD45.1-biotin, anti-Thy1.2-FITC, and isotype-matched mAbs were purchased from eBioscience (San Diego, CA). Anti-Arg-Biotin was purchased from Abcam (Cambridge, MA) and anti-iNOS-FITC was purchased from BD Biosciences (San Jose, CA). PKH26 was purchased from Sigma-Aldrich (St. Louis, MO). Flow cytometric analyses were performed using FACSCanto II and FACSDiVa software (BD Biosciences)

Isolation of monocytic MDSCs

BALB/c and C57BL/6 mice were injected subcutaneously with 5×10^5 MCA26 colon cancer cells and 5×10^5 Lewis lung carcinoma (LLC) cells, respectively. Mice were sacrificed when tumors reached $1\times1cm^2$. Splenocytes and bone marrow were processed to single cell suspensions. Red blood cells were lysed with ACK lysing buffer (Gibco; Carlsbad, CA). MDSCs were enriched by Percoll density gradient (GE Healthcare, UK). Fraction 2 ells were stained, in the presence of FcR blocking Ab, with Ly6C-FITC, bound to anti-FITC microbeads (Miltenyi; Auburn, CA), sorted via AutoMACS cell sorter (Miltenyi).

Mouse models of hepatic and lung metastases

MCA26 is a BALB/c-derived, chemically induced colon carcinoma with low immunogenicity (27). This cell was obtained from MD Anderson Cancer Center on 1994. It has been implanted in BABL/c mice. Our lab have routinely perform MHC class I, II staining and HLA typing and DNA fingerprinting using short tandem repeat to avoid contamination for every six to 12 months. Pathological analysis of tumor tissue had been preformed and diagnosed as colon adenocarcinoma at a regular basis during the experiments. A metastatic colon cancer model was generated as described previously (28). LLC is a C57BL/6-derived stable lung cancer cell line obtained from ATCC, 2011. Intrahepatic lung cancer metastases were similarly inoculated employing 7×10^4 LLC cells in C57BL/6 mice. Diffuse lung metastases wer generated with the injection of 2×10^5 LLC cells via tail vein. Pathological analysis had been preformed to confirm the lung adenocacinoma developed in the lung from experimental animals during the studies.

Cell Migration comparison

MDSCs were isolated as above from CD45.1 C57BL/6 mice. CIK cells were isolated per established protocols (29) from CD45.1 mice. Tumor-specific T-cells were isolated from the spleens of tumor bearing CD45.1 C57BL/6 mice via staining by anti-Thy1.2-FITC, and separated using anti-FITC microbeads via an AutoMACS cell sorter. Activated T-cells were isolated similarly and cultured in the presence of IL-2 (Peprotech; Rocky Hill, NJ) at 200 U/ml for 3 days. Macrophages were isolated by culturing bone marrow of naïve CD45.1 mice for 7 days in the presence of MCSF (Peprotech) at 30 ng/ml, followed by harvesting attached cells. Dendritic cells were generated by culturing bone marrow of naïve CD45.1 mice for 7 days in the presence of 1% GM-CSF conditioned medium (from J558L cell line) followed by harvesting nonadherent cells. Monocytes were isolated from percoll fraction 2 from the bone marrow of naïve CD45.1 mice. Cells were adoptively transferred, via tail

vein, to CD45.2 C57BL/6 mice bearing intrahepatic LLC tumors (14 days after tumor implantation). Mice were sacrificed after 72 hours for analysis.

Migration of PKH26-labeled cells

For PKH26 analysis, MDSCs were stained with PKH26 per manufacturer's instructions and adoptively transferred via tail vein into BALB/c mice bearing intrahepatic MCA26 colon cancer (14 days after inoculation). Organs were homogenized and immune cells were isolated, stained for MDSC markers, and analyzed by flow cytometry. Murine organs were also fixed with O.C.T. compound (Tissue-Tek; Torrence, CA), sectioned, and stained with Perl's Prussian blue to assess the presence of iron.

Feridex labeling and uptake

MDSCs were cocultured for 4 hours with Ferridex (ferumoxide, Berlex; Montville, NJ) at 11.2 mg/ml and sent to inductively coupled plasma mass spectrometry (ICP-MS, Cantest, Burnaby, BC) to determine total iron content. The percent Feridex uptake was then determined based upon the amount of iron detected in the cells by ICP-MS versus the total concentration of Feridex added during incubation. Cytospins were prepared by diluting 2×10^4 cells in 300 μL PBS. The cells were spun on glass slides using a Cytospin 3 centrifuge (Shandon, UK). Perl's Prussian blue staining was performed by fixing the samples with 4% paraformaldehyde for 10 minutes followed by incubation with 2% $K_3[Fe(CN)_6]$ in 2% HCl. Slides were counterstained with nuclear fast red and dehydrated in ethyl alcohol. Images were acquired with a Nikon microscope using specialized software (SOFT, Diagnostic Instruments, MI).

In vitro MRI of Feridex-labeled cells

Phantoms were prepared by adding known numbers of Feridex-labeled MDSCs into 0.2-ml 2% agrose gel, mixed, and snap frozen. Phantoms were imaged at 9.4 Tesla using a 89 mm bore system operating at a proton frequency of 400 MHz (Bruker Instruments, Billerica, MA). Multi-echo gradient echo (GRE) sequences were applied with the following parameters: TR=29.1ms, TE=5.1ms to 10 ms (n=5), 30 slices, flip angle=30°, number of signal averages (NEX)=8, in-plane resolution=0.098mm^2, and 100% z-rephasing gradient. R2*-maps were generated on a pixel-by-pixel basis using Matlab (R2007b; The Mathworks, Natick, MA). The signal intensity associated with each pixel was normalized to the standard deviation of adjacent noise prior to linear fitting of the signal-to-noise ratio versus echo time (TE). For the GRASP sequence the z-rephasing gradient was reduced to 50%.

In-vivo detection of Feridex-labeled cells by MRI

Tumor bearing BALB/c mice (n=7) were treated with 5×10^6 Feridex labeled MDSCs via tail vein. MR images of the liver, spleen, and tumor were obtained prior to injection and over 1 week post-injection. All *in vivo* MR imaging was performed as follows. Respiratory gating (SA Instruments, Inc., Stony Brook, NY) was employed. R2 and R2*-mapping was performed on a pixel-by-pixel basis using Matlab. To account for tumor growth over the 4-day interval, signal-to-noise ratios (SNR, where SNR=signal intensity divided by the standard deviation of the noise) were divided by the tumor area (mm^3) for all data obtained using GRE sequences. At various time points, representative mice were sacrificed, saline perfused, and their organs were harvested. A section of tissue was stained for iron using Perl's Prussian blue and the remaining tissue was re-weighed. The liver was sent to relaxometry and the tumor and spleen to ICP-MS for determination of iron content.

Relaxometry

Dose-response curves were generated by spiking ex-vivo tissue homogenate with known concentrations of Feridex (0–1 mM Fe, n=6). The transverse relaxation times (T2) were determined at 60 MHz (40° C) using a Bruker Minispec spectrometer (Bruker Medical GmbH, Ettlingen, Germany). T2 values were calculated based upon a mono-exponential fit of echo amplitude versus time.

Recombinant vesicular stomatitis virus vectors and transwell assay

The construction of rVSV-GFP and rVSV(MΔ51)-M3 have been described (30, 31). 1×10^4 tumor cells were cultured for 24 hours in the lower chamber of a 24 well transwell plate (Corning Costar). MDSCs were isolated as previously described and placed into VP-SFM medium (Gibco) on ice with rVSV-MDSC at various MOIs for 4 hours followed by thorough washing with cold medium. 1.5×10^5 cells were placed in the upper chamber of the same transwell plate (0.4μm pore size), incubated for 24 hours, and analyzed with a Leica DMRA2 fluorescent microscope.

Therapeutic Protocols

Eight-to-nine days after hepatic tumor implantation, when the tumor size reached 5×5–6×6mm^2, 5×10^6 monocytic MDSCs or Ly6C$^-$ cells passively loaded with rVSV-GFP in VP-SFM for 4 hours on ice at an MOI of 300 in the presence of polybrene (hexadimethrine bromide, Millipore; Billerica, MA), washed with ice cold PBS three times to remove free virus and then were injected via tail vein. 5×10^7 pfu rVSV-GFP was resuspended in 250μl PBS prior to transfer. Anti-VSV monoclonal antibody was incubated at 2 μg/ml on ice in the presence of rVSV-GFP or rVSV(MΔ51)-M3 (MOI:300) and polybrene for 1 hour, followed by addition of 5×10^6 MDSCs or Ly6C$^-$ cells and incubation on ice for an additional hour. Cells were washed three times with ice-cold PBS prior to transfer. Some mice were kept for survival and some were terminated at 96 hours after MDSC therapy and saved for histology, qPCR, $TCID_{50}$ and stained for VSV-G antigen (Alpha Diagnostic; San Antonio, TX).

FACS analysis of viral binding

2.5×10^5 MDSCs were combined with rVSV- GFP in the presence or absence of antibody as described above at viral MOIs of 0, 3, 10, 30, 100, 300, and 1000. Cells were left in culture at 37°C in RPMI for 72 hours prior to staining and flow cytometric analysis.

$TCID_{50}$ analysis of viral binding

Organs and cells were lysed, serially diluted and incubated with BHK21 cells at 37°C in VP-SFM medium for 72 hours. Cells were then examined under light microscopy for cytopathic effects (CPE). $TCID_{50}$ concentration was determined employing the Spearman-Karber method.

qPCR

RNA was isolated from organs using Trizol (Invitrogen; Carlsbad, CA) per manufacturer's specifications. qPCR was performed using RT^2 Real-Time SYBR Green/Rox PCR master Mix (SABiosciences; Frederick, MD) on an ABI PRISM 7900HT (Applied Biosystems; Foster City, CA) using the following primer sequences: 5′-TTCTTGGTTCTCCGAGTTGG-3′ and 5′-AACAGGAGGATGCAGCATTT-3′.

Cytotoxicity Assay

MDSCs cultured in the presence or absence of VSV-G Ab and rVSV(MΔ51)-M3 (MOI: 300) in the presence of polybrene as described above and coincubated with LLC tumor cells

at 12.5:1, 25:1, 50:1, and 100:1 for 4 hours. Supernatants were collected for measurement of Lactate Dehydrogenase release (CytoTox 96 Non-Radioactive Cytotoxicity Assay Kit; Promega, Madison, WI). Specific killing (in percentage) was calculated as experimental LDH release/maximum LDH release.

Statistical analysis

One-way ANOVA with Bonferroni post hoc tests was used to evaluate the significance associated with change in R2* as a function of time post Injection. Student's 1-sided t-test was used to compare the differences in tumor sizes and weights as well as FACS data, qPCR, and $TCID_{50}$ results. The log rank test was used to determine the significance of survival data.

Results

MDSCs exhibit stronger tumor-tropism than other immune cell types

In multiple murine models, MDSCs are present at high numbers at tumor sites (5, 6, 8, 11). We hypothesized that adoptive transfer of MDSCs should lead to preferential accumulation of MDSCs within tumor tissue, making them an excellent vector for oncolytic virus (OV) delivery. Previous studies have used different immune cell types for OV delivery, including TCR transgenic and IL-2 producing T-cells (25), cytokine induced killer cells (CIKs) (29, 32), as well as macrophages (26). In an attempt to determine which subset of cells possesses the strongest tumor tropism, we performed a series of experiments in which $CD45.1^+$ MDSCs, CIKs, tumor-specific T-cells, IL-2 activated T-cells, monocytes, macrophages, and dendritic cells were adoptively transferred into $CD45.2^+$ mice bearing intrahepatic LLC tumors, simulating metastatic lung cancer (Fig. 1). At 72 hours post-treatment, the mice were sacrificed and CD45.1 cells present in various organs were quantified. We observed a significantly higher number of MDSCs migrating to tumor-sites when compared to spleen and liver. We also found that MDSCs exhibited significantly greater tumor tropism than CIKs, activated T cells, normal T cells, monocytes, macrophages, and dendritic cells. The results suggest that MDSCs possess a greater potential for use in the delivery of tumor-specific therapies than other immune cell types analyzed.

Employing novel MRI techniques to track the kinetics of MDSC migration and localization in a hepatic tumor model

To determine the *in vivo* migration patterns of MDSCs longitudinally within individual mice, it is necessary to employ diagnostic imaging. Recently superparamagnetic iron oxide particles (SPIOs), such as Feridex, an SPIO currently used for *in vivo* clinical cell tracking, have been used to label multiple cell types for MRI detection (33, 34). This technique enables longitudinal tracking of SPIO-labeled MDSCs, as a function of time post-injection, without the need to sacrifice tumor-bearing mice. MRI also enables one to pinpoint the specific locations within each organ to which the labeled cells migrate.

MDSCs were isolated and purified from tumor-bearing mice (5). Greater than 96% of this population was $CD11b^+Gr\text{-}1^+$ (Supplemental Fig. 1), the classical markers of MDSCs. We created MRI phantoms of known iron and MDSC concentrations in agar and imaged via MRI (Supplemental Fig. 2a). These phantoms demonstrate a linear relationship between cell number and signal loss (Supplemental Fig. 2b). Prussian blue staining on cytospin samples confirmed the majority of MDSCs cocultured with Feridex stained positive for iron (Supplemental Fig. 2c), indicating that MDSCs can be effectively labeled with Feridex and imaged by MRI.

Feridex labeled MDSCs were administered to BALB/c mice previously implanted intrahepatically with MCA26 cells, simulating hepatic metastases of colon cancer. Mice received MRIs prior to adoptive transfer, then daily (n=7) for one week. Representative T2*-weighted images (GRE) and GRASP images are shown in Figure 2a and b at different magnifications. At 72 hours post-transfer, increased signal loss around the periphery and within vascular structures inside the tumor was observed. GRASP imaging has been developed to increase the accuracy of labeled cell detection (35) and a good correlation between GRE and GRASP is observed. The relative change in the R2* values, indicates maximum uptake of the cells into the lesion at 72 hours post-injection (Fig. 2c).

Mice were sacrificed at various time points and their organs were harvested. Iron concentration was quantified within tumor and spleen via mass spectrometry. Relaxometry, an NMR technique, which is able to distinguish superparamagnetic iron from physiologic iron, was then used to determine the Feridex concentrations within the liver tissue where there is a high concentration of endogenous iron (36). While iron levels were high in the tumor (38±2 %ID), minimal spleen (13±0.6 %ID) and liver uptake (0.5±1 %ID) was observed at 72 hours (Fig. 2d). Perl's staining was used to confirm the presence of iron in transferred cells within tumors at 72 hours post-injection (Fig. 2e). These methods reliably demonstrate that the adoptively transferred MDSCs targeted tumors, reaching peak concentrations 72 hours post-transfer, localizing peripherally and perivascularly, and some penetrating inside the tumor and intratumoral vasculature.

Confirmation of MRI findings through FACS analysis of PKH26 labeled MDSCs

We next employed flow cytometry to confirm the MRI findings. In this experiment, MDSCs were labeled with the membrane dye, PKH26, and adoptively transferred to BALB/c mice bearing intrahepatic MCA26 tumors. Representative mice were sacrificed each day and MDSC were re-isolated from liver, lungs, bone marrow, spleen, lymph nodes, blood, and tumors (Fig. 3a). FACS analysis demonstrated PKH26 signal increased in the tumor 4-fold over background at 48 hours after post-transfer, peaking at 8-times the background signal at 72 hours post-transfer (Fig. 3b, c). Little increase in PKH26 signal was observed in other organs. Notably, the liver showed no signal increase despite its proximity to the tumor. Circulating MDSCs decreased in correspondence to tissue dissemination, with blood levels reaching their nadir by 48 hours post-transfer (Fig. 3d).

Transfer of oncolytic viruses from MDSCs to tumor cells *in vitro* and *in vivo,* and prolonged survival in treated tumor-bearing mice

We next determined if MDSCs could effectively deliver OVs. MDSCs were incubated with rVSV-GFP, a VSV vector expressing green fluorescent protein (30), at varying MOIs. Free virus was washed away and cells were added to the upper chamber of a transwell plate, with MCA26 cells seeded in the lower chamber. After 24 hours, monolayers were examined for cytopathic effect (CPE) and GFP expression. MDSCs at all MOIs expressed high levels of GFP with minimal CPE, indicating that they had taken up and translated the viral genome without being lysed at 24 hours (Fig. 4a, 1st 2 columns). Tumor cells exhibited both CPE and GFP expression (Fig. 4a, columns 5 and 6). While GFP expression was high at all MOIs, CPE after 24 hours was most extensive at MOI 300. Similar results were obtained using 4T1 breast cancer and LLC cells, demonstrating applicability of VSV for multiple tumor models (Fig. 4a columns 3, 4 and 7, 8).

To test the efficacy and safety of VSV-MDSCs *in vivo,* we again employed the intrahepatic colon cancer model. Mice were injected with 5×10^6 VSV-MDSCs 8 days post-tumor implantation. Twelve days later, mice were sacrificed, and tumors measured and weighed.

Mice receiving VSV-MDSCs had significantly smaller tumors than controls, both dimensionally (Fig. 4b) and by weight (Fig. 4c).

To test whether VSV-MDSCs can maintain tumor-specificity, we repeated the previous migration experiment employing PKH26-labeled VSV-MDSCs. We were able to demonstrate a similar pattern of migration to tumors at 72 hours post-transfer, as seen with MDSCs lacking virus (Supplemental Fig. 3), indicating that infection of MDSCs with VSV does not alter their migratory kinetics.

Having demonstrated that VSV-MDSCs inhibit tumor growth, our next goal was to assess their effect on survival. Although there were no long-term survivors, the median survival in mice treated with VSV-MDSCs was significantly increased compared to controls (Fig. 4d). We also observed a survival advantage when comparing VSV-MDSC treated mice to those treated with MDSCs alone ($p<0.0002$) or Ly6C negative control cells loaded with VSV ($p<0.002$). This confirmed that the survival benefit was due to the tumor-targeting abilities of MDSCs and the oncolytic effects of VSV.

Finally we tested whether VSV-MDSCs were superior to a similar dose of peripherally-administered rVSV-GFP. Through $TCID_{50}$ assays, we determined the amount of VSV delivered by 5×10^6 VSV-MDSCs to be no greater than 5×10^7 $TCID_{50}$ of VSV (data not shown). Systemic administration of an equivalent dose of rVSV-GFP proved significantly inferior to VSV-MDSC treatment ($p<0.0001$).

The therapeutic efficacy of VSV-MDSC treatment using of a second-generation rVSV conjugated to MDSCs via a specific anti-VSV

In order to enhance viral loading of MDSCs, we tested whether a non-neutralizing monoclonal antibody directed against the VSV G-protein could enhance VSV binding by bridging the virus to the Fc receptors present on MDSCs.

We tested this theory by binding rVSV-GFP to the optimal amount of antibody followed by addition of MDSCs. When analyzed by FACS, MDSCs with antibody-bound virus demonstrated increased VSV staining (Fig. 5a) and GFP expression (Supplemental Fig. 4) compared to VSV-MDSCs generated by passive coupling at various MOIs. More importantly, significantly more VSV-positive cells were observed even when lower MOIs were used for the antibody-conjugated VSV-MDSCs ($p=0.003$; Fig. 5a). $TCID_{50}$ assays were performed on BHK-21 cells using VSV-MDSCs generated with or without antibody at a virus: MDSC ratio of 300. A 70-fold viral titer increase was observed when comparing antibody-conjugated VSV-MDSCs with passively-coupled VSV-MDSCs ($p<0.01$; Fig. 5b), thus confirming that significantly more VSV associates with the MDSCs through antibody conjugation.

We also sought to employ a second generation recombinant VSV to combat the robust host antiviral immune response, which limits viral replication in tumors. This recombinant VSV has been engineered to express the murine gammaherpes virus M3 protein, which binds a variety of chemokines with high affinity, leading to a significant delay in viral clearance (31). rVSV(MΔ51)-M3 (VSV(M3)) has also been engineered with an altered viral matrix protein, improving its safety profile by attenuating its ability to inhibit cellular protein synthesis, thus rendering the virus more susceptible to the interferon response of normal cells (19). There are no significant differences between these two forms of VSV in terms of viral replication (31).

We tested BALB/c mice bearing hepatic tumors with MDSCs conjugated to VSV(M3) via Fc receptor-bound anti-VSV (MDSC+Ab+VSV(M3)). MDSC+Ab+VSV(M3) treatment led

to long-term survival in 4 of 15 (26.3%) mice. The median survival following this treatment was significantly increased compared to PBS controls, $Ly6C^{-}$ cells antibody-conjugated to VSV(M3), or systemic injection of VSV(M3) (Fig. 5c). Mice treated with MDSC+Ab +VSV(M3) also survived significantly longer than mice treated with MDSCs antibody-conjugated to rVSV-GFP virus (MDSC+Ab+VSV(GFP)) as well as MDSCs passively conjugated with VSV(M3) (VSV(M3)-MDSC), indicating that enhanced survival can be attributed to both the improved viral vector and the improved viral loading onto MDSCs via antibody-conjugation. Similar therapeutic effects were obtained in a lung metastatic tumor model (Fig. 5d). In the lung metastasis model, we also observed an additive benefit for multiple injections of viral loaded MDSCs. Mice treated with 4 doses of MDSC+Ab +VSV(M3) survived significantly longer than mice administered the same treatment just once ($P = 0.008$). We also further confirm that MDSCs exposed to virus exhibited enhanced tumor killing when compared to those exposed solely to antibody alone. We concluded that the antibody did not affect MDSCs (supplementary Fig. 7). These results further support the utility of viral loaded MDSCs in treating multiples tumor types in various organs.

Confirmation of superior tumor-specific delivery of VSV-MDSCs compared to systemic viral therapy using immunohistochemical staining, $TCID_{50}$, and qPCR

To confirm that MDSC-mediated delivery of VSV exhibits greater tumor-specificity than systemic viral treatment, representative mice from each treatment group were sacrificed at 96 hours post-treatment and their tumors and organs were harvested. Staining for VSV-G was performed (Fig. 6a high power, Supplemental Fig. 5, low power). Tumors from mice treated with various MDSC-mediated therapies, including MDSC+Ab+VSV(M3), MDSC +Ab+VSV(GFP), and VSV(M3)-MDSCs, exhibited more extensive staining than tumors from controls or those treated with free virus. Necrosis was observed within the tumors of mice treated with MDSC+Ab+VSV(M3) but not other MDSC-targeted viral therapies, indicating that this method of treatment leads to the most robust tumor cell death at this time point. Intense staining was observed in the spleens and lungs, and to a lesser degree in the livers, from mice treated with free VSV(M3), but not in the mice treated with MDSC-targeted therapy. Central nervous tissue was also examined for VSV-G staining as a surrogate sign of potential neuropathic toxicity. Free VSV treatment resulted in brain positivity that was not demonstrated among MDSC-targeted VSV groups, indicating that MDSC-targeted therapy is safer than free virus therapy, likely due to the tumor-specific tropism of MDSCs and the inability of the MDSCs to cross the blood brain barrier. Pathologic examination of the central nervous tissue of mice in which long-term survival had been achieved demonstrated no abnormalities in the myelination, neuron density, or morphology of the cerebral cortex or cerebellar purkinje cell concentration within the cerebellum. In addition, there were no signs of ischemic damage or tissue necrosis (Supplemental Fig. 6).

To determine whether the positive staining represented viable VSV, organs from mice receiving free VSV(M3), VSV(M3)-MDSC, and MDSC+Ab+VSV(M3) were harvested and $TCID_{50}$ assays were performed (Fig. 6b). Tumors in mice receiving MDSC+VSV(M3) and MDSC+Ab+VSV(M3) demonstrated a significantly higher concentrations of virus than those receiving free VSV(M3). Further confirmation was demonstrated through qPCR of cell lysates from the organs of mice treated with free VSV(M3), MDSC+VSV(M3), and MDSC+Ab+VSV(M3) (Fig. 6c). Consistent with the $TCID_{50}$ assessment, tumors in mice receiving MDSC+VSV(M3) and MDSC+Ab+VSV(M3) demonstrated significantly more viral RNA than those receiving free VSV(M3) and MDSC+Ab+VSV(M3)-treated mice, viral RNA was more prevalent in tumors than in the spleens, livers, lungs, or brains. These may indicate the viral replication or more viruses taking up by the tumor due to the MDSC mediated oncolytic viral targeting.

MDSCs acquire an M1-like phenotype with inherent tumor killing ability upon exposure to VSV(M3)

MDSCs have classically been shown to promote an M2-like, pro-tumor environment. Recently, we demonstrated a plasticity in MDSC phenotype wherein, under certain conditions, MDSCs can exhibit M1-like characteristics (37). We used FACS to measure the M1 marker, inducible nitric oxide synthase (iNOS, Fig. 7a), and the M2 marker, arginase 1 (Arg, Fig. 7b), in MDSCs infected with VSV at various MOIs. Interestingly, iNOS positivity increased while Arg^+ cells decreased after culture with VSV(M3). We also observed an upregulation of iNOS in MDSCs exposed to antibody, virus, or both, and a significant downregulation of Arg in the presence of antibody and VSV(M3)(Fig. 7c).

To further demonstrate that MDSCs exposed to VSV(M3) exhibited an M1-like phenotype, we compared direct tumor lysis by unmanipulated MDSCs to those co-cultured with the anti-VSV Ab alone (MDSC+Ab), to VSV(M3)-MDSCs, or to MDSC+Ab+VSV(M3). We found that MDSCs, after viral exposure, efficiently killed tumor cells at multiple MDSC/tumor ratios (Fig. 7d). These data suggest that MDSCs, when exposed to virus, can switch from an M2 (Arg^+) to an M1-like phenotype ($iNOS^+$ and tumor lysis activity), which further promotes tumor killing.

Discussion

Previously, macrophages, T-cells, and NK cells have been employed as vectors for tumor-specific delivery of oncolytic virus (25, 26, 29, 32). Most of these immune cells migrate to lymphoid organs or to the liver (Fig. 1a). While OT-II (CD4 OVA-specific TCR transgenic) cells used as tumor-specific T cells worked well in a proof-of-principle study (25), for clinical use, generation and expansion of tumor specific T-cells is expensive and requires genetic manipulation (i.e. TCR transgene) making their use less practical. When comparing tumor-targeting ability, we found that MDSCs were superior to other immune cell types analyzed and exhibited more specific tropism. Moreover, we demonstrated that MDSCs penetrated into well-established tumors (tumors implanted for more than 14 days and larger than 1 cm^2) by multiple approaches, e.g. MRI and fluorescent labeling (Fig. 1 and 2). Most other immune cells tested preferentially migrated and homed to the spleen or liver.

$CD34^+$ mesenchymal stem cells (MSC) have also been used for tumor targeting. They migrate into lung, tumor, bone marrow, spleen and liver. Their use for the purpose of OV delivery proves problematic. Upon injection, MSC accumulate in the lung and do not migrate to tumors until 11 days after injection (40) at which time virally infected cells will likely have been cleared by the host immune response. Furthermore, MSC cannot efficiently penetrate into tumors and predominantly reside within the border zone of stromal cells and tumor tissues (41). Most importantly, MSC possess the ability to differentiate into different cell types, e.g. adipocyte, stromal fibroblast, osteoblasts et al., potentially facilitating tumor progression (40–42). In contrast, oncolytic virus loaded MDSC acquired M1-like antitumor phenotype without pro-tumor growth activity, and infiltrate tumors preferentially.

We demonstrated via MRI that MDSCs accumulated at the tumor periphery as well as perivascularly. To our knowledge, this is the first time the *in vivo* destination for MDSC migration has been demonstrated via direct imaging. The use of Feridex to image cell migration offers advantages over immunologic labeling techniques, including the ability to follow migration longitudinally in the same individual *in vivo,* which could translate well to humans. It has previously been shown that a single SPIO-labeled cell can be identified *in vivo* via MRI (38). However, with our equipment we are reliably able to detect 125 cells when identifying dendritic cells (36), which are similar in size to MDSCs, and appear to take up Feridex similarly based on our observations (data not shown). Due to its dextran coat,

Feridex remains intact and detectable longer than fluorescent labeling and its presence can be confirmed using ICP-MS, relaxometry, and histology. Feridex is also nontoxic and has been approved by the FDA for use in humans.

VSV therapy presents several unique challenges, which we attempted to overcome through the use of MDSCs as targeting vehicles, as well as through the use of a second generation VSV(M3) recombinant. Immune competent hosts are able to mount a rapid cellular immune response that halts viral replication after a few days. The oncolytic potency of VSV can be enhanced through vector-mediated inhibition of NK and NKT cells (39). By employing the VSV(M3) mutant, which has an altered matrix protein and expresses the murine gammaherpesvirus M3 protein, the virus replicates longer, resulting in a more potent oncolytic response (31). Unfortunately, VSV also harbors the risk of neuropathy, including paralysis or lethal encephalitis (22, 24, 31). What is intriguing with our treatment regimen is that none of the mice treated with VSV-MDSCs suffered from these effects. We confirmed histologically, as well as through $TCID_{50}$ assays, that the central nervous system of mice receiving VSV-MDSCs was relatively spared from VSV infection. Through tumor-specific viral targeting, we demonstrated that we could decrease the pharmacologic dose, thus increasing the therapeutic index. Importantly, the result also demonstrates a more widespread biological interest beyond the use of MDSC as carrier cells, i.e. the potential use of oncolytic viruses to modulate the immunosuppressive milieu within tumors.

While MDSCs have gained notoriety for their pro-tumor qualities, we have previously demonstrated the plasticity of their phenotype. Under certain conditions e.g. oncolytic viral activation, MDSCs can exhibit an anti-tumor, M1-like phenotype with tumoricidal activity (37), which may through the viral interaction with pattern recognition receptors (PRRs), e.g. TLR. One of our novel findings in this study is that, upon loading with oncolytic virus, MDSCs acquired an M1-like functional phenotype with direct tumor killing activity, thereby enhancing their ability to promote tumor regression without affecting their tumor tropism (Fig. 7a-d and Suppl. Fig. 3).

The identification of universal epitopes for the classification of human MDSCs has proven more challenging than for murine MDSCs. However, progress is being made toward finding a unified phenotype across a variety of cancer patients (16, 43–45). We have shown that MDSCs can be generated from murine embryonic and hematopoietic stem cells. From these data, it may be possible to generate or isolate MDSCs from the blood or bone marrow of cancer patients, arm these MDSCs with cancer-specific therapies, and transfer them back therapeutically.

In summary, both in humans and mice, MDSCs have been found to increase in the presence of virtually every form of cancer, including colon cancer (44), renal cell carcinoma (46), breast cancer (47), melanoma (44), and hepatocellular carcinoma (48). Despite their well-documented pro-tumor characteristics in tumor-bearing hosts, we demonstrated that MDSCs, when loaded with OV, can be used as a Trojan horse for the treatment of cancer and possibly a variety of other diseases.

Supplementary Material

Refer to Web version on PubMed Central for supplementary material.

Acknowledgments

The work was supported in part by grants from the National Cancer Institute, Black Family Stem Cell Foundation, and Pfizer research fund to S.-H. Chen, grant support from NCI and Susan G. Komen Breast Cancer Foundation to

P.-Y. Pan. We appreciate Mr. Boxun Xie for his preparation of the pathology slides and Dr. Mary Fowkes for her evaluation of histopathology.

References

1. Bronte V, Wang M, Overwijk WW, Surman DR, Pericle F, Rosenberg SA, et al. Apoptotic death of CD8+ T lymphocytes after immunization: induction of a suppressive population of Mac-1+/Gr-1+ cells. J Immunol. 1998; 161:5313–20. [PubMed: 9820504]
2. Bronte V, Chappell DB, Apolloni E, Cabrelle A, Wang M, Hwu P, et al. Unopposed production of granulocyte-macrophage colony-stimulating factor by tumors inhibits CD8+ T cell responses by dysregulating antigen-presenting cell maturation. J Immunol. 1999; 162:5728–37. [PubMed: 10229805]
3. Delano MJ, Scumpia PO, Weinstein JS, Coco D, Nagaraj S, Kelly-Scumpia KM, et al. MyD88-dependent expansion of an immature GR-1(+)CD11b(+) population induces T cell suppression and Th2 polarization in sepsis. J Exp Med. 2007; 204:1463–74. [PubMed: 17548519]
4. Youn JI, Nagaraj S, Collazo M, Gabrilovich DI. Subsets of myeloid-derived suppressor cells in tumor-bearing mice. J Immunol. 2008; 181:5791–802. [PubMed: 18832739]
5. Huang B, Pan PY, Li Q, Sato AI, Levy DE, Bromberg J, et al. Gr-1+CD115+ immature myeloid suppressor cells mediate the development of tumor-induced T regulatory cells and T-cell anergy in tumor-bearing host. Cancer Res. 2006; 66:1123–31. [PubMed: 16424049]
6. Dolcetti L, Peranzoni E, Ugel S, Marigo I, Fernandez Gomez A, Mesa C, et al. Hierarchy of immunosuppressive strength among myeloid-derived suppressor cell subsets is determined by GM-CSF. Eur J Immunol. 2009
7. Ozao-Choy J, Ma G, Kao J, Wang GX, Meseck M, Sung M, et al. The novel role of tyrosine kinase inhibitor in the reversal of immune suppression and modulation of tumor microenvironment for immune-based cancer therapies. Cancer Res. 2009; 69:2514–22. [PubMed: 19276342]
8. Pan PY, Wang GX, Yin B, Ozao J, Ku T, Divino CM, et al. Reversion of immune tolerance in advanced malignancy: modulation of myeloid-derived suppressor cell development by blockade of stem-cell factor function. Blood. 2008; 111:219–28. [PubMed: 17885078]
9. Cheng P, Corzo CA, Luetteke N, Yu B, Nagaraj S, Bui MM, et al. Inhibition of dendritic cell differentiation and accumulation of myeloid-derived suppressor cells in cancer is regulated by S100A9 protein. J Exp Med. 2008; 205:2235–49. [PubMed: 18809714]
10. Gabrilovich D, Ishida T, Oyama T, Ran S, Kravtsov V, Nadaf S, et al. Vascular endothelial growth factor inhibits the development of dendritic cells and dramatically affects the differentiation of multiple hematopoietic lineages in vivo. Blood. 1998; 92:4150–66. [PubMed: 9834220]
11. Bunt SK, Sinha P, Clements VK, Leips J, Ostrand-Rosenberg S. Inflammation induces myeloid-derived suppressor cells that facilitate tumor progression. J Immunol. 2006; 176:284–90. [PubMed: 16365420]
12. Sawanobori Y, Ueha S, Kurachi M, Shimaoka T, Talmadge JE, Abe J, et al. Chemokine-mediated rapid turnover of myeloid-derived suppressor cells in tumor-bearing mice. Blood. 2008; 111:5457–66. [PubMed: 18375791]
13. Ochoa AC, Zea AH, Hernandez C, Rodriguez PC. Arginase, prostaglandins, and myeloid-derived suppressor cells in renal cell carcinoma. Clin Cancer Res. 2007; 13:721s–6s. [PubMed: 17255300]
14. Capuano G, Rigamonti N, Grioni M, Freschi M, Bellone M. Modulators of arginine metabolism support cancer immunosurveillance. BMC Immunol. 2009; 10:1. [PubMed: 19134173]
15. Corzo CA, Cotter MJ, Cheng P, Cheng F, Kusmartsev S, Sotomayor E, et al. Mechanism regulating reactive oxygen species in tumor-induced myeloid-derived suppressor cells. J Immunol. 2009; 182:5693–701. [PubMed: 19380816]
16. Hoechst B, Ormandy LA, Ballmaier M, Lehner F, Kruger C, Manns MP, et al. A new population of myeloid-derived suppressor cells in hepatocellular carcinoma patients induces CD4(+)CD25(+)Foxp3(+) T cells. Gastroenterology. 2008; 135:234–43. [PubMed: 18485901]
17. Pucci F, Venneri MA, Biziato D, Nonis A, Moi D, Sica A, et al. A distinguishing gene signature shared by tumor-infiltrating Tie2-expressing monocytes, blood “resident” monocytes, and embryonic macrophages suggests common functions and developmental relationships. Blood. 2009; 114:901–14. [PubMed: 19383967]

18. Yang L, DeBusk LM, Fukuda K, Fingleton B, Green-Jarvis B, Shyr Y, et al. Expansion of myeloid immune suppressor Gr+CD11b+ cells in tumor-bearing host directly promotes tumor angiogenesis. Cancer Cell. 2004; 6:409–21. [PubMed: 15488763]

19. Stojdl DF, Lichty B, Knowles S, Marius R, Atkins H, Sonenberg N, et al. Exploiting tumor-specific defects in the interferon pathway with a previously unknown oncolytic virus. Nat Med. 2000; 6:821–5. [PubMed: 10888934]

20. Thomsen AR, Nansen A, Andersen C, Johansen J, Marker O, Christensen JP. Cooperation of B cells and T cells is required for survival of mice infected with vesicular stomatitis virus. Int Immunol. 1997; 9:1757–66. [PubMed: 9418136]

21. Huang TG, Ebert O, Shinozaki K, Garcia-Sastre A, Woo SL. Oncolysis of hepatic metastasis of colorectal cancer by recombinant vesicular stomatitis virus in immune-competent mice. Mol Ther. 2003; 8:434–40. [PubMed: 12946316]

22. Ebert O, Harbaran S, Shinozaki K, Woo SL. Systemic therapy of experimental breast cancer metastases by mutant vesicular stomatitis virus in immune-competent mice. Cancer Gene Ther. 2005; 12:350–8. [PubMed: 15565179]

23. Jenks N, Myers R, Greiner SM, Thompson J, Mader EK, Greenslade A, et al. Safety studies on intrahepatic or intratumoral injection of oncolytic vesicular stomatitis virus expressing interferon-beta in rodents and nonhuman primates. Hum Gene Ther. 2010; 21:451–62. [PubMed: 19911974]

24. Plakhov IV, Arlund EE, Aoki C, Reiss CS. The earliest events in vesicular stomatitis virus infection of the murine olfactory neuroepithelium and entry of the central nervous system. Virology. 1995; 209:257–62. [PubMed: 7747478]

25. Qiao J, Kottke T, Willmon C, Galivo F, Wongthida P, Diaz RM, Thompson J, Ryno P, Barber GN, Chester J, Selby P, Harrington K, Melcher A, Vile RG. Purging metastases in lymphoid organs using a combination of antigen-nonspecific adoptive T cell therapy, oncolytic virotherapy and immunotherapy. Nat Med. 2008; 14:37–44. [PubMed: 18066076]

26. Muthana M, Giannoudis A, Scott SD, Fang H-Y, Coffelt SB, Morrow FJ, et al. Use of Macrophages to Target Therapeutic Adenovirus to Human Prostate Tumors. Cancer Research. 2011; 71:1805–15. [PubMed: 21233334]

27. Corbett TH, Griswold DP Jr, Roberts BJ, Peckham JC, Schabel FM Jr. Tumor induction relationships in development of transplantable cancers of the colon in mice for chemotherapy assays, with a note on carcinogen structure. Cancer Res. 1975; 35:2434–9. [PubMed: 1149045]

28. Caruso M, Pham-Nguyen K, Kwong YL, Xu B, Kosai KI, Finegold M, et al. Adenovirus-mediated interleukin-12 gene therapy for metastatic colon carcinoma. Proc Natl Acad Sci U S A. 1996; 93:11302–6. [PubMed: 8876130]

29. Thorne SH, Negrin RS, Contag CH. Synergistic Antitumor Effects of Immune Cell-Viral Biotherapy. Science. 2006; 311:1780–4. [PubMed: 16556847]

30. Ebert O, Shinozaki K, Huang TG, Savontaus MJ, Garcia-Sastre A, Woo SL. Oncolytic vesicular stomatitis virus for treatment of orthotopic hepatocellular carcinoma in immune-competent rats. Cancer Res. 2003; 63:3605–11. [PubMed: 12839948]

31. Wu L, Huang TG, Meseck M, Altomonte J, Ebert O, Shinozaki K, et al. rVSV(M Delta 51)-M3 is an effective and safe oncolytic virus for cancer therapy. Hum Gene Ther. 2008; 19:635–47. [PubMed: 18533893]

32. Kottke T, Diaz RM, Kaluza K, Pulido J, Galivo F, Wongthida P, et al. Use of biological therapy to enhance both virotherapy and adoptive T-cell therapy for cancer. Mol Ther. 2008; 16:1910–8. [PubMed: 18827807]

33. Arbab AS, Yocum GT, Kalish H, Jordan EK, Anderson SA, Khakoo AY, et al. Efficient magnetic cell labeling with protamine sulfate complexed to ferumoxides for cellular MRI. Blood. 2004; 104:1217–23. [PubMed: 15100158]

34. Beduneau A, Ma Z, Grotepas CB, Kabanov A, Rabinow BE, Gong N, et al. Facilitated monocyte-macrophage uptake and tissue distribution of superparmagnetic iron-oxide nanoparticles. PLoS One. 2009; 4:e4343. [PubMed: 19183814]

35. Mani V, Briley-Saebo KC, Itskovich VV, Samber DD, Fayad ZA. Gradient echo acquisition for superparamagnetic particles with positive contrast (GRASP): sequence characterization in

membrane and glass superparamagnetic iron oxide phantoms at 1.5T and 3T. Magn Reson Med. 2006; 55:126–35. [PubMed: 16342148]

36. Briley-Saebo K, Bjornerud A, Grant D, Ahlstrom H, Berg T, Kindberg GM. Hepatic cellular distribution and degradation of iron oxide nanoparticles following single intravenous injection in rats: implications for magnetic resonance imaging. Cell Tissue Res. 2004; 316:315–23. [PubMed: 15103550]
37. Ma G, Pan P-Y, Eisenstein S, Divino CM, Lowell CA, Takai T, et al. Paired Immunoglobin-like Receptor-B Regulates the Suppressive Function and Fate of Myeloid-Derived Suppressor Cells. Immunity. 2011; 34:385–95. [PubMed: 21376641]
38. Hinds KA, Hill JM, Shapiro EM, Laukkanen MO, Silva AC, Combs CA, et al. Highly efficient endosomal labeling of progenitor and stem cells with large magnetic particles allows magnetic resonance imaging of single cells. Blood. 2003; 102:867–72. [PubMed: 12676779]
39. Altomonte J, Wu L, Meseck M, Chen L, Ebert O, Garcia-Sastre A, et al. Enhanced oncolytic potency of vesicular stomatitis virus through vector-mediated inhibition of NK and NKT cells. Cancer Gene Ther. 2009; 16:266–78. [PubMed: 18846115]
40. Nakamura K, Ito Y, Kawano Y, Kurozumi K, Kobune M, Tsuda H, et al. Antitumor effect of genetically engineered mesenchymal stem cells in a rat glioma model. Gene Ther. 2004; 11:1155–64. [PubMed: 15141157]
41. Serakinci N, Christensen R, Fahrioglu U, Sorensen FB, Dagnaes-Hansen F, Hajek M, et al. Mesenchymal stem cells as therapeutic delivery vehicles targeting tumor stroma. Cancer Biother Radiopharm. 2011; 26:767–73. [PubMed: 21877908]
42. Djouad F, Plence P, Bony C, Tropel P, Apparailly F, Sany J, et al. Immunosuppressive effect of mesenchymal stem cells favors tumor growth in allogeneic animals. Blood. 2003; 102:3837–44. [PubMed: 12881305]
43. Liu CY, Wang YM, Wang CL, Feng PH, Ko HW, Liu YH, et al. Population alterations of L: -arginase- and inducible nitric oxide synthase-expressed CD11b(+)/CD14 (−)/CD15 (+)/CD33 (+) myeloid-derived suppressor cells and CD8 (+) T lymphocytes in patients with advanced-stage non-small cell lung cancer. J Cancer Res Clin Oncol. 2009
44. Mandruzzato S, Solito S, Falisi E, Francescato S, Chiarion-Sileni V, Mocellin S, et al. IL4Ralpha+ myeloid-derived suppressor cell expansion in cancer patients. J Immunol. 2009; 182:6562–8. [PubMed: 19414811]
45. Rodriguez PC, Ernstoff MS, Hernandez C, Atkins M, Zabaleta J, Sierra R, et al. Arginase I-producing myeloid-derived suppressor cells in renal cell carcinoma are a subpopulation of activated granulocytes. Cancer Res. 2009; 69:1553–60. [PubMed: 19201693]
46. Ko JS, Zea AH, Rini BI, Ireland JL, Elson P, Cohen P, et al. Sunitinib mediates reversal of myeloid-derived suppressor cell accumulation in renal cell carcinoma patients. Clin Cancer Res. 2009; 15:2148–57. [PubMed: 19276286]
47. Diaz-Montero CM, Salem ML, Nishimura MI, Garrett-Mayer E, Cole DJ, Montero AJ. Increased circulating myeloid-derived suppressor cells correlate with clinical cancer stage, metastatic tumor burden, and doxorubicin-cyclophosphamide chemotherapy. Cancer Immunol Immunother. 2009; 58:49–59. [PubMed: 18446337]
48. Hoechst B, Voigtlaender T, Ormandy L, Gamrekelashvili J, Zhao F, Wedemeyer H, et al. Myeloid derived suppressor cells inhibit natural killer cells in patients with hepatocellular carcinoma via the NKp30 receptor. Hepatology. 2009; 50:799–807. [PubMed: 19551844]

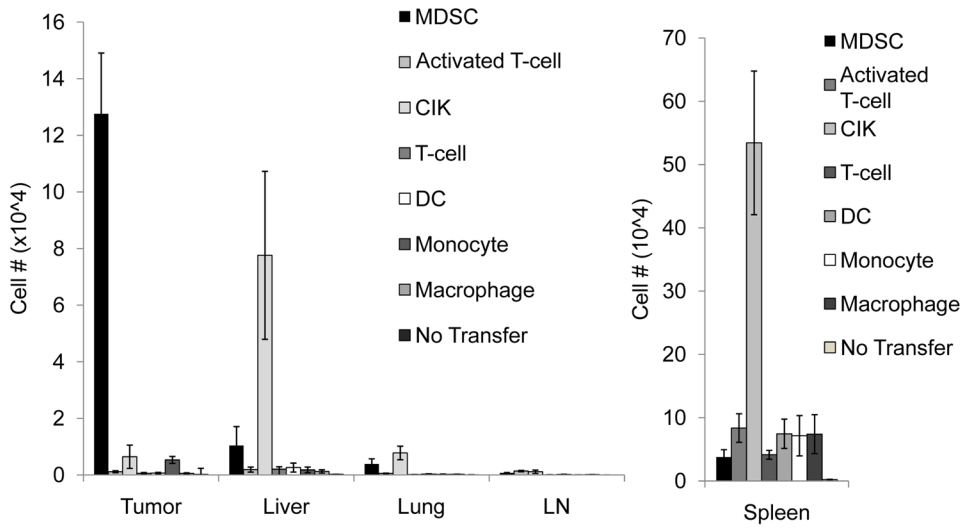

Figure 1. MDSCs exhibit stronger tumor tropism than other immune cell types

CD45.1 Ly6C$^+$ MDSCs (MDSC), Cytokine-induced killer cells (CIK), activated T-cells (aT-cells), tumor-specific T-cells (T-cells), macrophages, monocytes, dendritic cells (DC), were transferred to mice bearing intrahepatic LLC tumors. Mice that did not receive cell transfer (No tx) were used as controls. Mice were sacrificed at 72 hours. Organs were harvested and the presence of CD45.1 cells was determined by FACS. Tumors from mice receiving MDSCs demonstrated a significantly greater CD45.1$^+$ population than spleen or liver ($1.28\pm0.215\times10^5$ vs. $3.78\pm1.17\times10^4$ ($p=0.03$) and $1.04\pm0.671\times10^4$ ($p=0.0003$)). Tumors from mice receiving MDSCs had a larger CD45.1$^+$ population than those from mice injected with other cell types: CIKs ($6.45\pm4.12\times10^3$, $p=0.001$), aT-cells ($1.13\times10^3\pm350$, $p=0.0009$), T-cells (603 ± 244, $p=0.0008$), monocytes ($5.32\pm1.23\times10^3$, $p=0.001$), macrophages (546 ± 197, $p=0.0008$), and dendritic cells (666 ± 239, $p=0.005$).

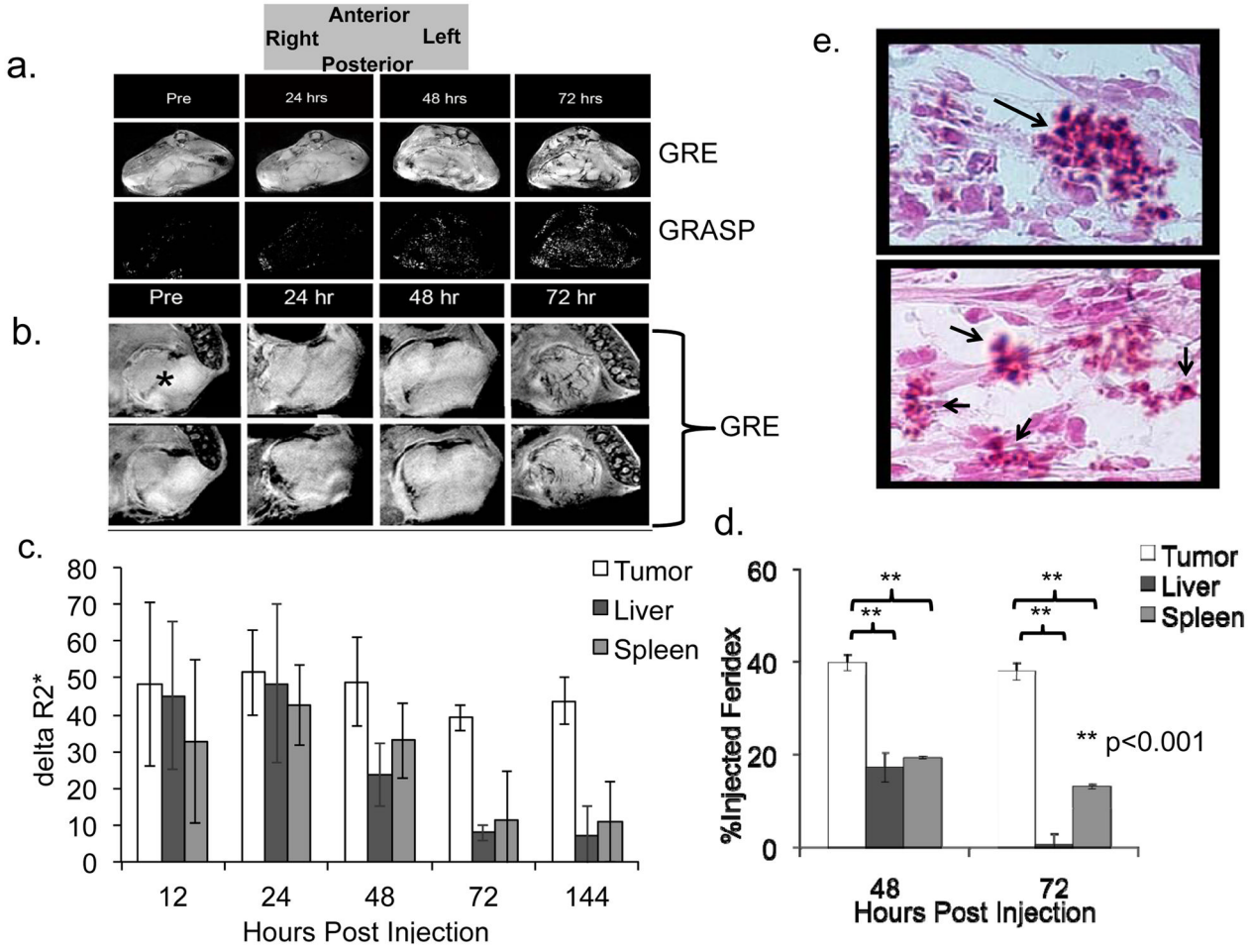

Figure 2. The use of MRI to follow *in vivo* migration of adoptively transferred MDSCs to tumor sites

Feridex labeled Ly6C$^+$ MDSCs were transferred to mice bearing intrahepatic MCA26 tumors in their livers (n=7). **a)** Representative T2-weighted images of the entire mouse cross section are shown from prior to adoptive transfer (pre) and then daily post-transfer, up to 4 days, in both GRE (upper panels) and GRASP (lower panels) modalities. **b)** Representative close-up view of the tumor section reveals signal loss in multiple cuts peripherally as well as in a vascular distribution at 72 hours after transfer (GRE: black; GRASP: white; *= tumor). **c)** MRI data was then analyzed and R2* quantification was performed pixel-by-pixel in order to quantify signal loss as a function of time. Data is presented as an increase in signal loss over baseline (pre-transfer values) at the designated time points. **d)**. Mice were sacrificed, saline perfused, and tumor, liver and spleen were removed. The presence of Feridex was shown to be significantly higher in the tumor than the spleen via ICP-MS (40±2 % Injected Dose (ID) vs. 19±0.3 %ID, 48hrs and 38±2 %ID vs. 13±0.6 %ID, 72hrs) as well as in the liver via relaxometry (0.5±1 %ID, 72hrs) and results were compared to the known amount of Feridex injected into the mice based on the standard curve determined in Suppl. Figure 2b (**p<0.001). **e)** Tumors were resected 72 hours post transfer and stained with Perl's Prussian blue to indicate the presence of Iron oxide (positive results indicated by arrows).

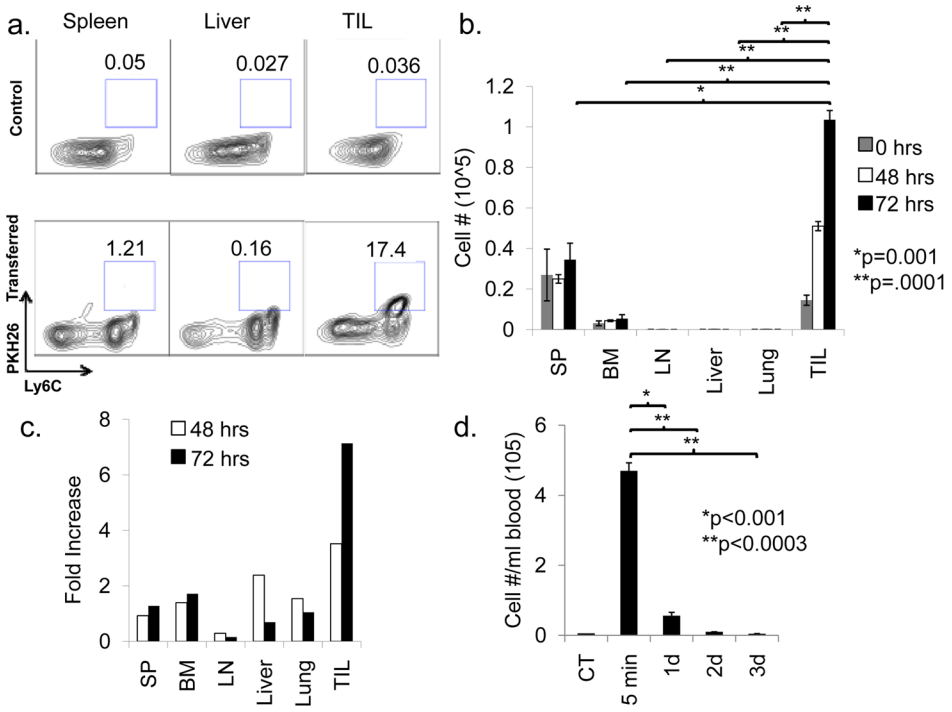

Figure 3. Confirmation of MDSC migration to tumor sites by flow cytometric analysis

PKH26-labeled Ly6C$^+$ MDSCs were transferred to mice bearing MCA26 tumors in their livers. Representative mice were sacrificed each day for 3 days and spleen, bone marrow, lymph nodes, liver, lung, and tumor were resected, and homogenized. Immune cells were isolated by Percoll fractionation, stained with antibodies against Ly6C, and analyzed via FACS for PKH26 positivity (n=3 per time point). **a)** Representative FACS plots are shown comparing the spleens, livers, and tumors (tumor-infiltrating leukocyte, TIL) from tumor-bearing mice receiving no MDSC transfer (control, upper panels) to those from tumor-bearing mice sacrificed 3 days after PKH26-labeled MDSC transfer (3 Day, lower panels). **b)** The total number of MDSCs present was determined for each of the harvested organs. **c)** Data is also displayed as fold-increase over background signal (based on mice that did not receive PKH26 labeled cells). **d)** The number of circulating labeled MDSCs was also determined by sacrificing representative mice at the designated time points followed by cardiac aspiration. Leukocytes were prepared and the total number of Ly6C$^+$PKH26$^+$ cells was determined by flow cytometric analysis (n=3 per time point).

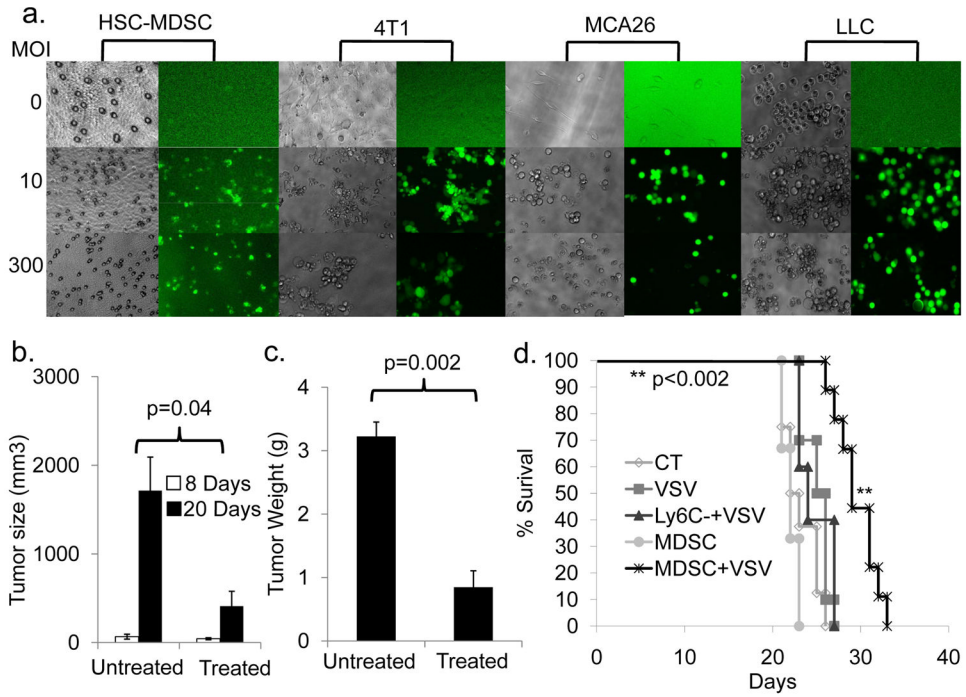

Figure 4. VSV-loaded MDSCs can transfer virus to tumor cells, leading to smaller tumor sizes and prolonged survival

a) Ly6C^{+} MDSCs were passively loaded with VSV-GFP (VSV-MDSC) at the specified MOI and placed in the upper chamber of a transwell plate with MCA26 tumor cells seeded in the lower chamber. Cells were incubated for 24 hours and examined under light (1st and 3rd columns) and fluorescent (2nd and 4th columns) microscope for cytopathic effects and GFP expression. **b, c)** VSV-MDSCs (MOI: 300) were injected into MCA26 tumor-bearing mice. Mice were sacrificed 12 days later. Tumors were resected, measured (**b**; p=0.04), and weighed Mice receiving VSV-MDSCs had significantly smaller tumors than controls, both dimensionally **b)** 410 mm^3 vs. 1710 mm^3; p=0.04 and by weight **c)** 0.85g vs. 3.22g; p=0.002. **d)** Intrahepatic MCA26 tumor-bearing mice were followed for survival after treatment with VSV-MDSCs (MOI: 300; n=9). Mice receiving VSV-MDSCs lived significantly longer than mice receiving PBS injection alone (29.8 days vs. 23 days, p<0.0004; n=8), MDSCs alone (p<0.002, n=3), the Ly6C^{-} cell fraction, acquired during MDSC isolation and passively loaded with VSV at MOI: 300 (p<0.002, n=5), or an equivalent amount of free VSV-GFP virus (p<0.0001; n=10).

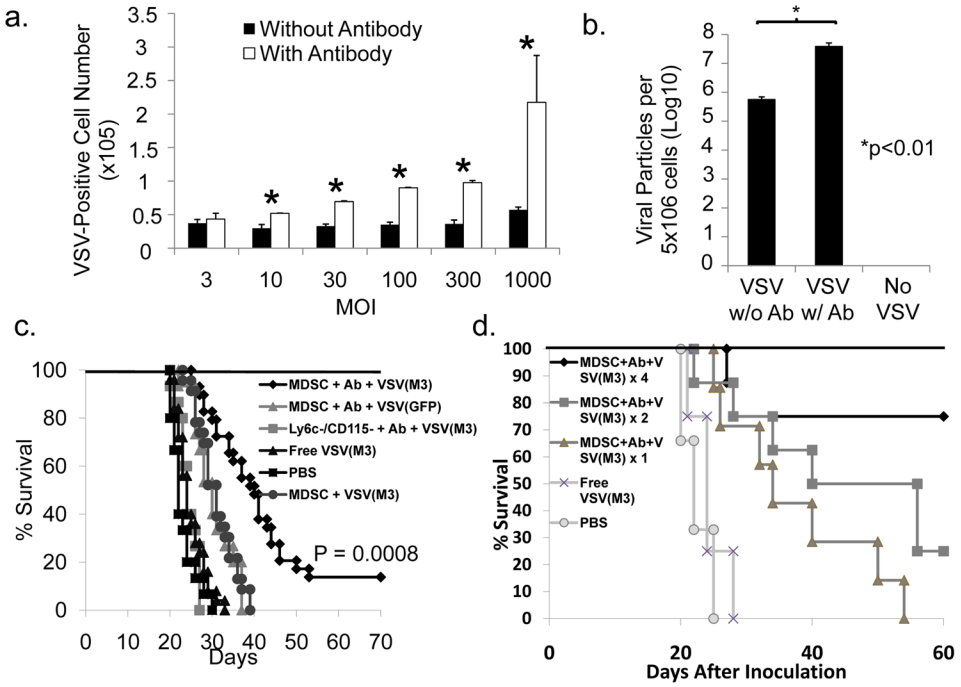

Figure 5. Antibody conjugation and use of VSV(M3) improves viral delivery to tumor sites and prolongs survival in tumor-bearing mice

a) VSV-GFP was incubated with anti-VSV antibody or isotype control. VSV-Ab mixture was added to MDSCs at designated MOIs and cultured for 72 hours, followed by VSV-G staining and FACS analysis. Cells with Ab conjugated virus showed significantly higher levels of VSV staining: 2.98×10^4 vs. 5.20×10^4 of VSV-G^+ cells at MOI: 10, p=0.001; 3.28×10^4 vs. 6.95×10^4 MOI:30, p<0.0001; 3.51×10^4 vs. 9.00×10^4 MOI:100, p<0.0001; 3.62×10^4 vs. 9.77×10^4 MOI:300, p<0.0001; 5.72×10^4 vs. 2.17×10^5 MOI:1000, p=0.008. **b)** MDSCs were treated as in **a**) at an MOI=300 and were lysed and cultured with BKH21 cells for 72 hours followed by assessment of CPE and $TCID_{50}$.. Ab conjugation significantly increased the viral delivery by MDSC. **c)** Intrahepatic MCA26 tumor-bearing mice were followed for survival after treatment with MDSCs+Ab+VSV(M3) (MOI: 300; n=15). Mice receiving MDSC+Ab+VSV(M3) lived significantly longer than those treated with PBS (n=15, median survival = 52.9 days vs. 24.6d p<0.0001). They also survived longer than mice treated with the $Ly6C^-$ cells conjugated to VSV(M3) at MOI: 300 (p<0.0001, n=15); an equivalent amount of free VSV(M3) virus (p<0.0001; n=15); VSV(M3)-MDSCs (p<0.0001; n=15), and MDSC+Ab+VSV- GFP (p=0.0009; n=15). **d)** C57BL6 mice were inoculated with 2×10^5 LLC cells via tail vein. Ten days after inoculation, mice were randomized to the following treatment groups: MDSC+Ab+VSV(M3) four times, MDSC +Ab+VSV(M3) twice, MDSC+Ab+VSV(M3) once, Free VSV(M3) or PBS. Treatments were administered on day 10 and subsequently at 3-day intervals for groups receiving multiple injections. MDSC conjugation to viral particles was performed as previously described. Four doses of MDSC+Ab+VSV(M3) significantly prolonged the survival when compared to treatment with PBS (P = 0.0004), Free VSV(M3) (P = 0.003), or one dose of MDSC+Ab+VSV(M3) (P = 0.008).

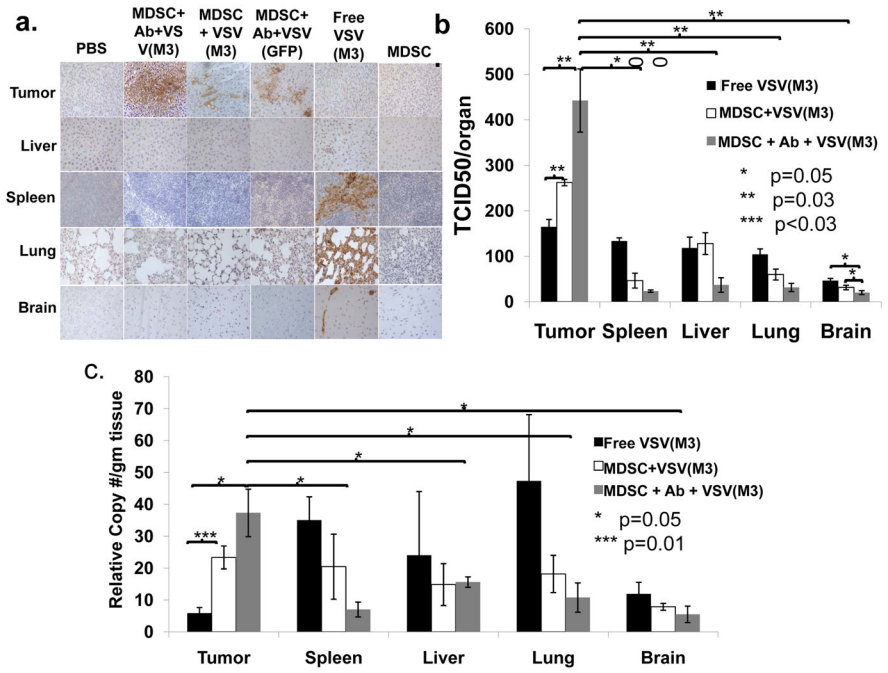

Figure 6. VSV-MDSCs exhibit greater tumor specificity than free virus

a) Mice bearing intrahepatic MCA26 tumors were treated with (from left to right): PBS, MDSC+Ab+VSV(M3), MDSCs passively loaded with VSV(M3)-MDSC without antibody (MDSC+VSV(M3)), MDSC+Ab+VSV-GFP, free VSV(M3), and MDSCs alone. Mice were sacrificed 96 hours after treatment. Organs were harvested and stained for VSV-G (brown). Organs stained include (top to bottom): tumor, liver, spleen, lung, and brain (40× magnification). MDSC- targeted therapy resulted in stronger VSV-G expression in the tumor. The mice treated with free VSV(M3) demonstrated strong VSV-G staining in spleen, liver, and lung. Free virus treated mice also exhibited some staining within the brain tissue, not seen in mice treated with MDSC-targeted VSV. **b)** Organs of mice treated as in **a)** were homogenized and $TCID_{50}$ were assessed. **c)** The RNA was isolated and analyzed for VSV-G by qPCR. Mice treated with MDSC+Ab+VSV(M3) demonstrated significantly more virus and viral RNA in the tumor than in other organs as well as more virus and viral RNA in the tumor than in mice treated with VSV-MDSCs or free virus (*p=0.05, **p=0.03, ***p=0.01)

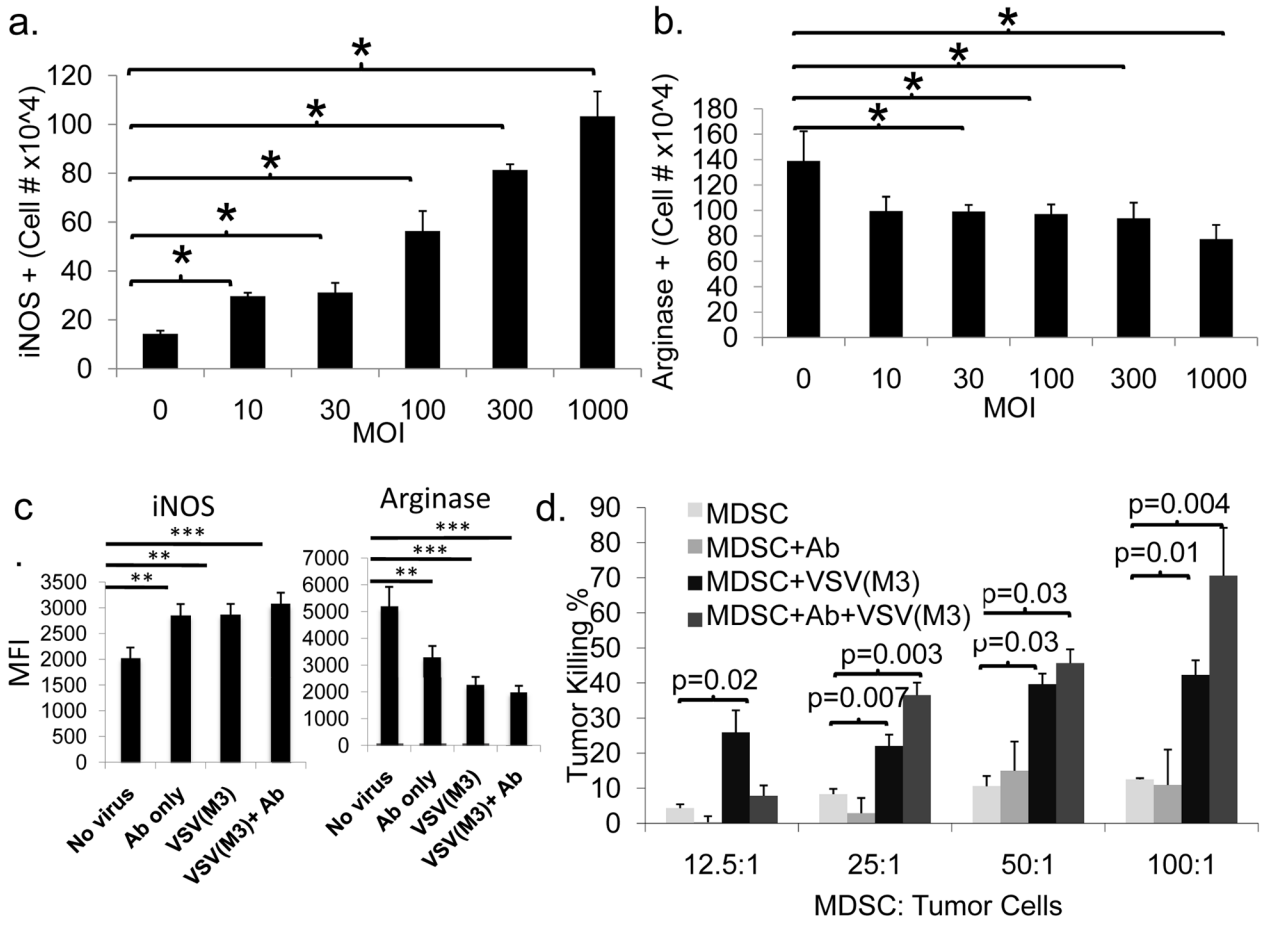

Figure 7. Exposure of MDSCs to VSV(M3) promotes acquisition of M1-like characteristics

a, b) Unmanipulated MDSCs or MDSCs incubated with Ab+VSV(M3) were subjected to intracellular staining for iNOS and arginase 1 (Arg). Infection with VSV led to a significant increase in the number of $iNOS^+$ cells ($3.0\pm0.14\times10^4$ cells at an MOI of 10 and $1.0\pm0.1\times10^5$ cells at an MOI of 1000 vs. $1.4\pm0.13\times10^4$ cells without infection, $p<0.0002$ and $p=0.0001$). Conversely, infection with VSV caused a decrease in Arg^+ cells from $1.3\pm0.23\times10^5$ in the absence of infection to $9.9\pm0.52\times10^4$ at an MOI of 10 ($p=0.04$), down to $7.7\pm1.1\times10^4$ at an MOI of 1000 ($p=0.01$). **c)** MDSCs were left untreated or incubated with Ab, VSV(M3), or Ab+VSV(M3) for 48 hours followed by intracellular staining for iNOS and Arg. MDSCs incubated with Ab, VSV(M3) or Ab+VSV(M3) showed increased expression of iNOS and decreased expression of Arg when compared to untreated MDSCs. **d)** MDSCs from **c** were co-cultured with LLC tumor cells in various ratios (MDSC:tumor cells = 12.5:1, 25:1, 50:1,100:1) for 4 hours. Tumor cell killing was assessed by determination of LDH release. VSV-MDSC and MDSC+Ab+VSV(M3) demonstrated significantly increased tumor killing effects.